LJMU Research Online

Sakaris, C, Bashir, M, Yang, Y, Michailides, C, Wang, J and Sakellariou, J

 Diagnosis of damaged tendons on a 10 MW multibody floating offshore wind turbine platform via a response-only Functional Model Based Method

http://researchonline.ljmu.ac.uk/id/eprint/15076/

Article

For more information please contact researchonline@ljmu.ac.uk

Diagnosis of damaged tendons on a 10 MW multibody floating offshore wind turbine platform via a response-only Functional Model Based Method

Christos S. Sakaris [a], Musa B. Bashir [a,*], Yang Yang [a], Constantine Michailides [b], Jin Wang [a],

John S. Sakellariou [c]

[a] *Department of Maritime and Mechanical Engineering, Liverpool John Moores University, Liverpool, Byrom Street, L3 3AF, UK*

[b] *Department of Civil Engineering and Geomatics, Cyprus University of Technology, 2-8 Saripolou, 3036 Limassol, Cyprus*

[c] *Department of Mechanical Engineering & Aeronautics, University of Patras, GR 26504 Patras, Greece*

Abstract: The problem of damaged tendon diagnosis (damage detection, damaged tendon identification and damage precise quantification) in a new multibody offshore platform supporting a 10 MW Floating Offshore Wind Turbine (FOWT) is investigated for the first time in this study. Successful operation of the multibody FOWT depends on the integrity of its tendons connecting the upper and lower tanks of the platform. Thus, early diagnosis of the damaged tendons is of high importance and it is achieved through a vibration-based methodology. Damage detection is accomplished based on the detection of changes in the vibration response power spectral density, while damaged tendon identification and damage precise quantification are accomplished through the Functional Model Based Method (FMBM). The FMBM is appropriately formulated in this study to operate with only vibration response signals. The employed vibration responses under healthy and damaged states of the FOWT platform are obtained from a numerical model describing the platform's dynamics. Each examined damage scenario corresponds to the reduced tendon's stiffness at the connection point to the platform's upper tank. Subtle damages corresponding to a stiffness reduction of [10-25] %, have

---

[*] Corresponding author: m.b.bashir@ljmu.ac.uk

minor effects on the platform's dynamics due to the tendons' high strength and damages corresponding to a stiffness reduction of [10-85] % have similar effects thus leading to a highly challenging diagnosis. The use of a single underwater accelerometer as well as a low and limited frequency bandwidth of surge acceleration signals, is explored. The results show that effective, reliable and very quick damaged tendon diagnosis can be achieved by a vibration-based methodology using the multibody FOWT platform's dynamics under damaged tendons.

Key words: Damaged tendon diagnosis, Structural Health Monitoring, Functional Models, Statistical time series methods, Floating Offshore Wind Turbine platform, Station-keeping of offshore platform

1.　Introduction

A new multibody offshore platform to support a 10 MW Floating Offshore Wind Turbine (FOWT), has been proposed by Esteyco (Armesto et al. 2018) for the ARCWIND project. The platform consists of an upper tank (providing buoyancy) and a lower tank (for ballasting). The two tanks are connected by tendons (steel cables) which are critical in maintaining the stability of the FOWT (Yang et al. 2020a). Early diagnosis of damaged tendons (damage detection, damaged tendon identification, damage quantification) is vital, as this is associated with a reduction in the maintenance costs and the efficient operation of the wind turbine. As in offshore structures supported by Tension Leg Platforms (Ren and Zhou 2012, Jahangiri et al. 2016, Wang et al. 2018), failure to diagnose damaged tendons early could lead to increase in the tendons' tension, thus resulting in the loss of stability of the structure and potentially leading to its collapse. Yet, the problem of damaged tendon diagnosis in the 10 MW multibody FOWT platform, has not been investigated. However, damaged tendon diagnosis (Ettefagh 2015, Jahangiri et al. 2016, Chandrasekaran and Chithambaram 2019) and damaged mooring line diagnosis (Jamalkia et al. 2016, Begg et al. 2018, Wang et al. 2018, Chandrasekaran and Chithambaram 2018, Tang et al. 2020) on offshore structures have been investigated in a limited number of studies using vibration based structural health monitoring methods. These methods operate in very small

and low frequency bandwidths and they may be distinguished into two broad families according to the employed models, namely, *physics–based models* or *data-based models*.

In the first family, *physics–based models* of the structural dynamics are employed and damage detection (Ettefagh 2015, Begg et al. 2018), damaged tendon identification (Ettefagh 2015), damaged mooring line identification (Begg et al. 2018) and damage quantification (Ettefagh 2015, Begg et al. 2018) are treated as an inverse problem where information extracted from measured signals is used to reconstruct the mass, stiffness and damping of the system. Yet, a detailed model representing the structural dynamics is required for the effectiveness of these methods (Ettefagh 2015). Moreover, the solution of the inverse problem and the identification of a damage may not always be possible due to potential ill conditioning problems (Begg et al. 2018).

In the second family, *data-based models* developed exclusively through measured signals from the structure, are employed. In the context of these methods, damage detection (Jahangiri et al. 2016, Jamalkia et al. 2016, Tang et al. 2020), damaged tendon identification (Jahangiri et al. 2016), damaged mooring line identification (Jamalkia et al. 2016) and damage quantification (Jahangiri et al. 2016, Jamalkia et al. 2016) are treated as a classification problem where an unknown state is roughly classified as the healthy state or as a pre-specified damaged state of specific type and magnitude. In particular studies such as Chandrasekaran and Chithambaram 2018, 2019, damage detection is achieved based on the detection of dissimilarities between the raw signals obtained from the healthy state and an unknown state of the structure, and damaged tendon identification is achieved through the identification of the damaged tendon as the tendon closest to the sensor providing the greatest dissimilarities. Also, the solution of the classification problem requires multiple sensors such as 6 sensors in Jamalkia et al. (2016). The increased damage severity often leads to mis-classifications as some of the frequencies move toward other frequencies due to the change of damage intensity thus leading to specific and limited frequency variations (Jamalkia et al. 2016).

The treatment of damage quantification as a classification problem is much simpler than damage precise quantification which requires the estimation of the damage precise magnitude in any continues range of

magnitudes. Obviously, for quantification of high accuracy based on the classification treatment, a high number of prespecified damage magnitudes is required and they are often not available in practice.

Damage precise quantification has been investigated through the development of a vibration-based method, the Functional Model Based Method (FMBM), which has been applied only in an aircraft skeleton and a railway vehicle (Sakellariou and Fassois 2008, Kopsaftopoulos and Fassois 2013, Sakellariou et al. 2015). The FMBM is equipped with stochastic, data-based, Functional Models (FMs) which are of advanced statistical time series type with parameters functionally (pseudo-statically) dependent upon the proper operating parameter (Sakellariou and Fassois 2008, Kopsaftopoulos and Fassois 2013, Sakellariou et al. 2015, Sakellariou and Fassois 2016, 2017). Based on the vibration signals from a proper sample of damage magnitudes and the representation of damage magnitude by the operating parameter, the FM model is able to represent the partial structural dynamics for any damage magnitude in any continues range of magnitudes. Apart from providing the precise magnitude of a damage, the FMBM also provides the corresponding uncertainty interval for the estimated magnitude thus accounting for certain additional uncertainties. The only FMs which have been used for damage precise quantification, are the Functionally Pooled AutoRegressive with eXogenous excitation (FP-ARX) model and its' extension, the Vector FP-ARX model, which are estimated based on the excitation and response signals (Sakellariou and Fassois 2008, Kopsaftopoulos and Fassois 2013, Sakellariou et al. 2015, Sakellariou et al. 2018). The FMBM have been also used for damage precise localization which requires the precise estimation of the damage locations' Cartesian coordinates (Kopsaftopoulos and Fassois 2013, Sakaris et al. 2015, 2016, 2017a, 2017b, Sakellariou et al. 2018).

The problem of damaged tendon diagnosis in the 10 MW multibody FOWT platform, is investigated for the first time in the present study through a vibration-response-only based methodology. Damage detection is achieved through a statistical hypothesis testing procedure based on the Power Spectral Density (PSD) of vibration response signals. Damaged tendon identification and damage precise quantification are achieved through the FMBM (Sakellariou and Fassois 2008) which is appropriately formulated in this study to operate with only vibration response signals. The FMBM is equipped with a Functionally Pooled AutoRegressive (FP-

AR) model which is exclusively based on response signals.

The employed vibration responses under healthy and different potential damaged states of the FOWT platform, are obtained from a numerical model describing the platform's dynamics. As this is an early study on damaged tendon diagnosis on a new 10 MW multibody FOWT platform, the platform is investigated under parked conditions only. Thus, this coupled model of two rigid tanks and 6 flexible tendons (Yang et al. 2020a, 2020b) is subjected only to current and irregular wave excitation loads (Chen and Basu 2019). The loads are based on the characteristics of the most severe environmental conditions of a selected site located at Scotland's northern coast. Each examined damage scenario corresponds to the reduction in a tendon's stiffness (%) at the connection point of the tendon to the platform's upper tank. Two of the total six tendons are examined in this study, the tendon which sustains the largest tension due to its proximity to the wave direction and another tendon selected randomly from the tendons not being close to a mooring line. Examined damages corresponding to a stiffness reduction of [10-25] %, have minor effects on the platform's dynamics due to the tendons high strength and damages corresponding to a stiffness reduction of [10-85] %, affect similarly the dynamics. Thus, the diagnosis capability of the methodology is tested under highly challenging conditions. A number of practical constraints are explored in this study such as the use of a single underwater accelerometer thus keeping the hardware and wiring complexity low. Additionally, the diagnosis is achieved within a limited and low frequency bandwidth as it is necessary due to the physical excitation under the actual operating conditions. Although a single underwater sensor placed on the upper tank is used to measure the six degrees of freedom accelerations, only the surge acceleration is employed as the effects of the considered damages on the PSD estimates of the surge acceleration are more significant.

The rest of this article is structured as follows: The FOWT platform, the tendon damages and the simulation details are presented in Section 2. The methodology for damaged tendon diagnosis is presented in Section 3. The damaged tendon diagnosis results are presented in Section 4. The conclusions are summarized in Section 5.

2.   The structure, the dynamics, the damage scenarios and the simulations

2.1   The structure

The examined structure in this study is a new multibody floating platform (called TELWIND platform) developed by Esteyco to support a 10 MW FOWT in the ARCWIND project (Yang et al. 2020a). The 10 MW multibody FOWT platform consists of a ballasting lower tank (LT) and an upper tank (UT) connected through 6 tendons (steel cables), with the UT providing buoyancy while the LT ensures stability. A telescopic tower is incorporated in the platform with a view to easing the transport and installation processes (Figure 1). The tanks are made of concrete in order to reduce the cost. The fairleads of the mooring lines are attached to the top surface of the UT which is 10 m below the mean sea level. The UT is 10 m below the mean sea level (MSL) with a draught of 16.75 m. The LT has a draught of 22.5 m and the total draught of the combined structure is 92.25 m. The diameters of UT and LT are 44.5 m and 23.0 m, respectively. Each of the tendons has a length of 48.81 m and an equivalent diameter of 0.271 m (for more information see Yang et al. 2020a).

2.2   The damage scenarios

Each examined damage scenario corresponds to the reduction in a tendon's stiffness (%) at the connection point of the tendon to the upper tank of the platform. Two of the total 6 tendons are examined in this study. These are, tendon 5 which sustains the largest tension due its proximity to the wave direction (Yang et al. 2020a) and tendon 2 which is randomly selected from other tendons not in close proximity to a mooring line (Figure 1). Each examined single damage is designated as F_m^q with $q = 2, 5$ for the examined tendon and m is the damage magnitude (% stiffness reduction). It is noted that these tendons play significant role in the stability of the 10 MW FOWT platform, as they are capable of undermining the platform's stability if the ballasting lower tank loses its connection to the upper structures.

2.3   The simulations

The vibration responses under healthy and different potential damaged states of the 10 MW multibody
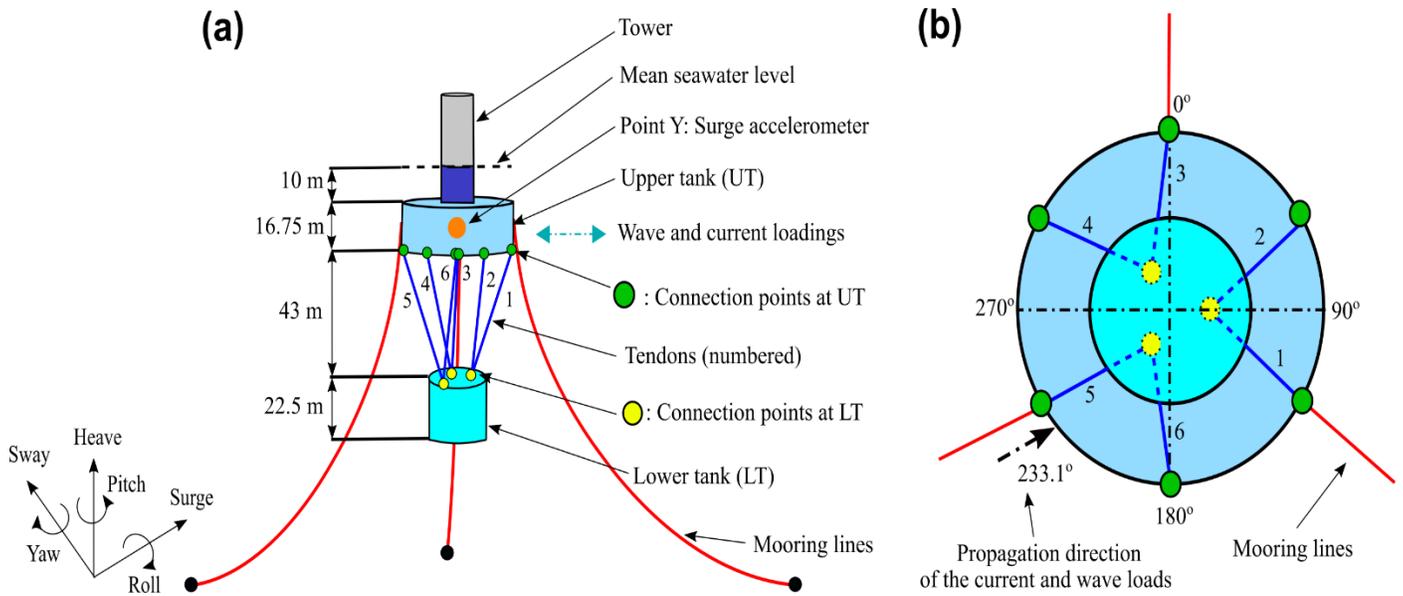
Figure 1. (a) The 10 MW multibody FOWT platform, the position of the accelerometer (Point Y) and the damage locations which are the connection points at the UT. (b) Bottom view of the platform with the propagation direction of the current and wave excitation loads.

FOWT platform, are obtained from a numerical model describing the platform's dynamics. As this is an early study on damaged tendon diagnosis on the new 10 MW multibody FOWT platform, the platform is firstly investigated under parked conditions. Thus, the platform is modeled as coupled, consisting of two rigid tanks (UT and LT), three mooring lines and 6 flexible tendons subjected only to current and irregular wave excitation loads. Although the tendons on this platform are designed to be remain tension in order to provide the required stability, it is noted that the effects of wave-current interaction on its loadings can cause complex hydrodynamic consequences that include displacement of spectral frequency and shapes (Chen and Basu 2019). The effect of wind is neglected because the study only focused on the parked conditions. The resulting impact of mooring line behaviors on the structural responses of the platform is considered in the simulations. The mooring lines are modelled as a nonlinear catenary in the prediction of the coupled dynamic responses of the platform. The method used in the modelling based on a concept proposed by Chen et. al. 2018.

A modal analysis of the healthy platform obtains 6 modes and 4 eigenfrequencies 0.027 Hz, 0.228 Hz, 0.325 Hz, 0.874 Hz which are presented in Figure 2. It is noted that the local roll – pitch modes and the roll - pitch

modes have a repeated eigenfrequency of 0.874 Hz and 0.027 Hz, respectively. Consequently, a comparison of PSD estimates via the Welch estimator (Stoica and Moses 1997, pp. 52 - 53) (Welch estimation details: Matlab function *pwelch.m*; signal length 20000 samples, window length 868 samples, 95 % overlap, Hamming window, frequency resolution of 0.011 Hz) of roll and pitch acceleration signals corresponding to the healthy state and for hydrodynamic damping ratios of 4 %, 6 %, 8 %, 10 %, 12 %, 14 %, is presented in Figure 3. It is observed that the first peak of the roll/pitch PSDs is at 0.023 Hz and the last peak at 0.86 Hz for all the considered hydrodynamic damping ratios and these peaks correspond to the roll/pitch mode (with eigenfrequency of 0.027 Hz) in Figure 2 and the local roll/pitch mode (with eigenfrequency of 0.874 Hz). This indicates that hydrodynamic damping does not affect the modes which have a repeated eigenfrequency and thus this eigenfrequency is independent of the hydrodynamic damping.
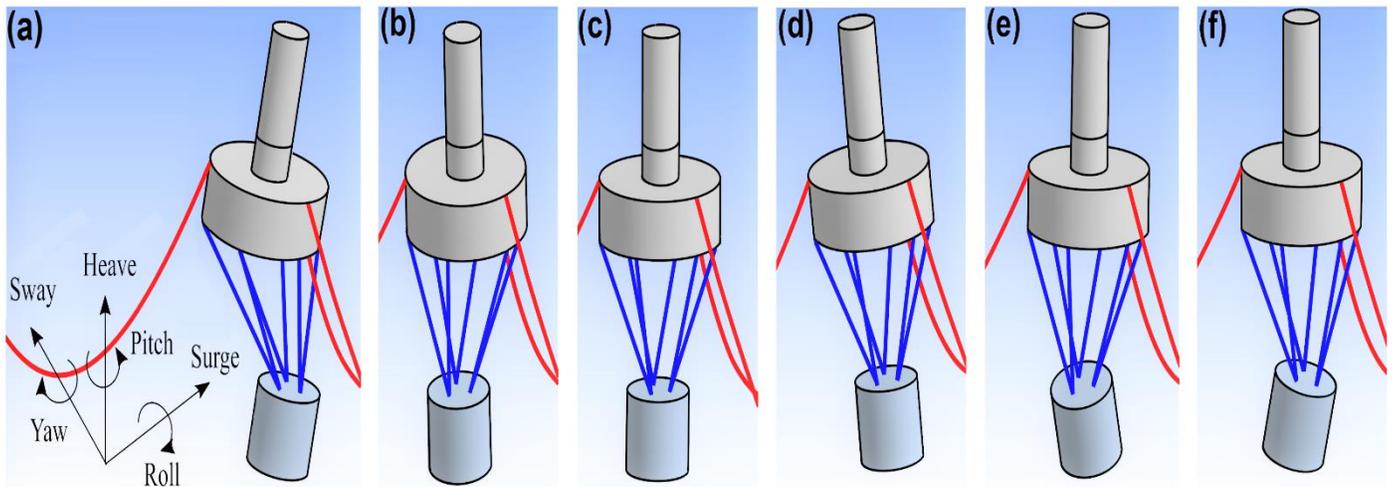
Figure 2. Modes from the numerical model of the FOWT platform. (a) Local-pitch mode (with eigenfrequency 0.874 Hz) based on the pitch movement of both tanks. (b) Local-roll mode (with eigenfrequency 0.874 Hz) based on the roll movement of both tanks. (c) Local-yaw mode (with eigenfrequency 0.228 Hz) corresponding to the twist of the tendons. (d) Pitch mode (with eigenfrequency 0.027 Hz) based on the pitch movement of the platform. (e) Roll mode (with eigenfrequency 0.027 Hz) based on the roll movement of the platform. (e) Local-pitch mode (with eigenfrequency 0.325 Hz) based on the pitch movement of the lower tank. (f) Local-roll mode (with eigenfrequency 0.325 Hz) based on the roll movement of the lower tank.

The numerical model is constructed in AQWA which is a component of the commercial software package ANSYS. The 3D diffraction and radiation theory is applied for the prediction of the current and irregular wave excitation loads on the platform. The panel model of the platform is established in AQWA for frequency domain analysis. The mesh of the model is presented in Figure 4. The maximum mesh size is 1.1 m and the amount of the diffraction elements is 8902. Further details on the platform properties have been presented in Yang et al. 2020a, 2020b. In the frequency domain analysis, 35 wave headings with an interval of 10 degree are examined. The examined wave frequency bandwidth is [0.0016-0.484] Hz. The excitation wave loads, added mass and radiation damping are then obtained and used for time domain analysis. In each time domain simulation, the duration and time step are 12300 s and 0.1 s, respectively. In order to avoid the transient effects in the results, only the results after 1500 s in the simulations are used for damaged tendon diagnosis.
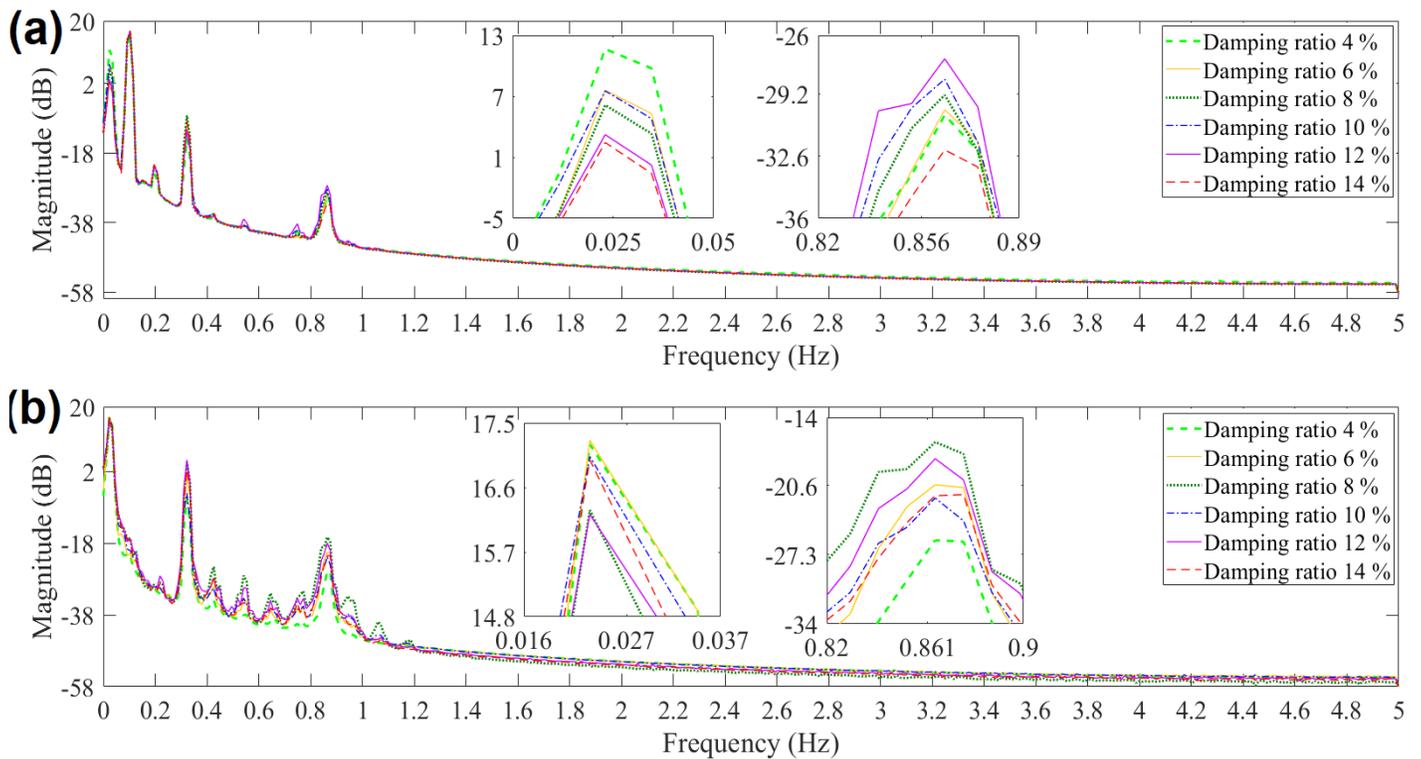
Figure 3. Welch-based PSD estimate of (a) pitch and (b) roll acceleration signals for the healthy state under hydrodynamic damping ratios 4 %, 6 %, 8 %, 10 %, 12 %, and 14 %.

Irregular waves are used because they constitute a realistic representation of open sea conditions (Journee

and Massie 2001, p. 25). An irregular wave is the linear combination of regular waves which are sinusoidal waves with different heights and frequencies (Faltinsen 1990, pp. 37, 39). The irregular wave is generated based on the modified two-parameter Pierson-Moskowitz spectrum (Journee and Massie 2001, pp. 40-41, Chakrabarti 2005, pp. 106-108) given in Equation (1).
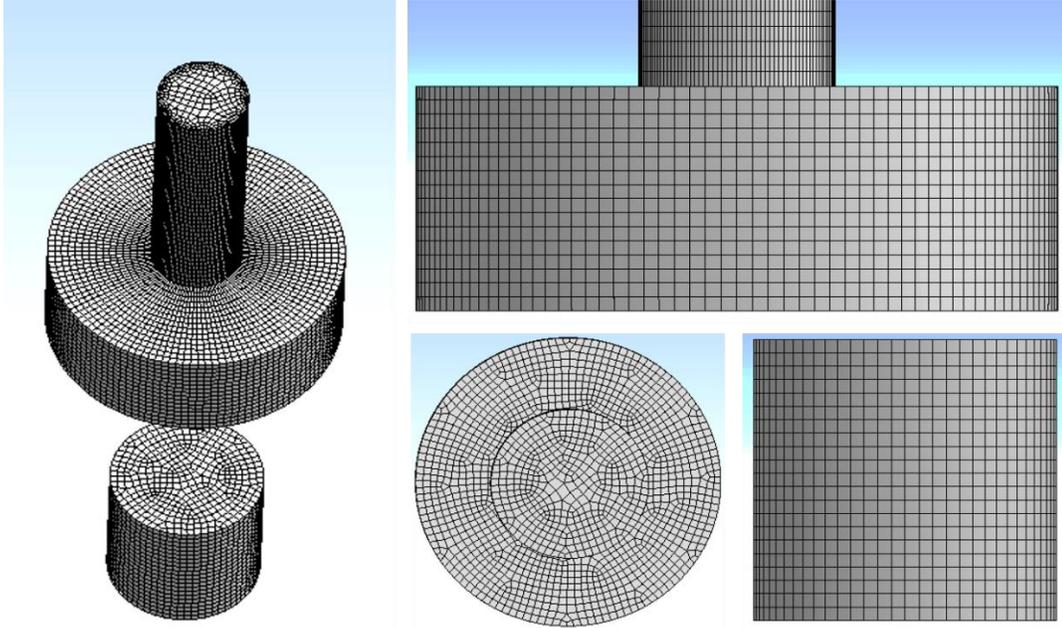
Figure 4. Panel mesh of the numerical model of the 10 MW multibody FOWT platform.

$$S(f_c) = 2\pi S(\omega_c) = 2\pi S(2\pi f_c) = 2\pi \frac{5}{16} H_s \frac{(2\pi f_o)^4}{(2\pi f_c)^5} e^{-1.25(\frac{2\pi f_c}{2\pi f_o})^{-4}} \tag{1}$$

where $S(f_c)$ and $S(\omega_c)$ are the PSDs at frequency f_c (Hz) and ω_c (rad/sec) respectively, H_s (m) is the significant wave height and f_o (Hz) is the peak frequency corresponding to the significant wave height. The generation of an irregular wave is based on an excitation bandwidth $f_c \in [0.1\text{-}100]$ Hz, a peak frequency f_o = 0.10 Hz and a significant wave height H_s = 5 m. The considered propagation direction of the current and wave loads is 233.1° (Figure 1(b)) whereas the speed of the current at mean sea level is 0.22 m/s. The details

of the current and wave excitation loads are based on the characteristics of the most severe environmental conditions of the selected site located in the northern coast of Scotland.

The six degrees of freedom (surge, heave, sway, roll, yaw and pitch) accelerations are measured using a single underwater sensor placed on the UT (Point Y, Figure 1(a)). However only the surge acceleration is used in this study because it is judged as the most dominant through the investigation on the effects induced by the magnitudes of responses from other degrees of freedom on the PSD estimates of the considered damage scenarios. The acceleration signals are sampled at $f_s = 10$ Hz (acceleration signal bandwidth $f_a \in [0–5]$ Hz) with each being $N = 20000$ samples (2000 s) long.

6 acceleration signals are obtained from each simulation, one for each degree of freedom. A total of 4 simulations are conducted with the healthy structure and 128 with a single damage of each of the 19 considered magnitudes at each of the 2 considered damage locations (connection points of tendons 2, 5 at the UT, see Figure 1). 2 simulations with the healthy structure and 20 simulations with the damaged structure (one per damage magnitude, covering the range [10, 100] % with a step of 10 %, in each of the two tendons) are used for the training of the methodology. The remaining simulations with the healthy structure and 108 with the damaged structure (3 simulations for each damage magnitude, covering the range of [10, 95] % with a step of 5 %, in each of the two tendons) are solely used in the inspection phase for the methodology's performance assessment. Each signal is sample mean corrected and scaled by its sample standard deviation. The details on the simulations and measured signals are presented in Table 1.

2.4 Effects of damage on the dynamics of FOWT platform

A PSD estimate (Welch estimation details: Matlab function *pwelch.m*; signal length 20000 samples, window length 868 samples, 95 % overlap, Hamming window, frequency resolution of 0.011 Hz) is provided in Figure 5 and it corresponds to the healthy state. In this PSD estimate, the first highest peak at 0.1066 Hz is due to the irregular wave with a peak frequency $f_o = 0.1$ Hz. The second highest peak at 0.864 Hz is due to the local-pitch or the local-roll mode (with eigenfrequency 0.874 Hz; Figure 2) corresponding to the pitch or roll

movement of both tanks respectively. The pitch and roll modes have equal response characteristics due to symmetry of the model along longitudinal and transverse axes. The third highest peak at 0.23 Hz is due to the local-yaw mode (with eigenfrequency 0.228 Hz) corresponding to the twist of the tendons. The fourth highest peak at 0.034 Hz is due to the pitch or roll mode (with eigenfrequency 0.027 Hz) corresponding to the pitch or roll movement of the platform respectively. The fifth highest peak at 0.322 Hz is due to the local-pitch or the local-roll mode (with eigenfrequency 0.325 Hz) corresponding to the pitch or roll movement of the lower tank respectively.

Table 1. Details of the performed simulations and vibration signals.

Structural state	Description	No. of damaged tendons	No. of damage magnitudes	No. of simulations – Baseline phase	No. of simulations – Inspection phase
Healthy	-		-	2	3
Damaged	Reducing the stiffness of a single tendon (%) (step of 5%)	2 (Tendons 2, 5)	19	20 (one per damage magnitude [10, 20, 30, 40, …., 100] % on each tendon)	108 (3 per damage magnitude [10, 15, 20, 25, …., 95] % on each tendon)

Sampling frequency: $f_s = 10$ Hz, acceleration signal bandwidth: $f_a \in$ [0-5] Hz

Signal length: $N= 20000$ samples (2000 s)
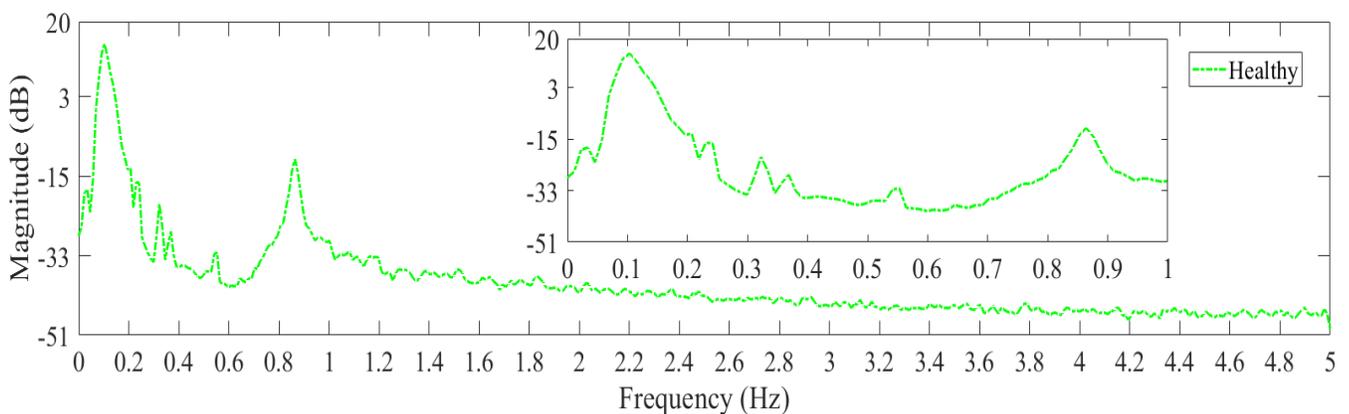
Figure 5. Welch-based PSD estimate and a blow-up of it for the healthy state.

In Figure 6, the effects of selected damage scenarios on the structural dynamics are shown via Welch-based (Welch estimation details: Matlab function *pwelch.m*; signal length 20000 samples, window 868 samples, 95

% overlap, Hamming window, frequency resolution of 0.011 Hz) PSD estimates corresponding to the healthy structure and the structure under 14 damage scenarios (magnitudes). Figures 6(a)-(c) depict the PSDs corresponding to the healthy structure and the damage scenarios $F_{10}^2, F_{20}^2, F_{30}^2, F_{40}^2, F_{50}^2, F_{60}^2$, and F_{70}^2. Figures 6(d)-(f) depict the PSDs corresponding to the healthy structure and the damage scenarios $F_{10}^5, F_{20}^5, F_{30}^5, F_{40}^5$, $F_{50}^5, F_{60}^5,$ and F_{70}^5. Based on the bandwidths of [0.27-0.35] Hz and [0.7-0.9] Hz where two structural modes are included, it is observed that the damages $F_{30}^2, F_{40}^2, F_{50}^2, F_{60}^2, F_{70}^2, F_{30}^5, F_{40}^5, F_{50}^5, F_{60}^5,$ and F_{70}^5 affect significantly the structural dynamics (big discrepancies from the healthy PSD with frequency shifts up to 0.17 Hz) and thus it is expected of the platform's stability to be affected as well. Furthermore, it is evident that the effects of the damages $F_{10}^2, F_{20}^2, F_{10}^5,$ and F_{20}^5 on the platform are insignificant (small discrepancies from the healthy PSD with frequency shifts around of 0.012 Hz) due to the tendons high strength. This also indicates that these damages are small and that damaged detection is challenging.

An additional comparison between the Welch-based (Welch estimation details: Matlab function *pwelch.m*; signal length 20000 samples, window 868 samples, 95 % overlap, Hamming window, frequency resolution of 0.011 Hz) PSD estimates for some of the considered damage scenarios, is shown in Figure 7. For each pair of the compared damage scenarios (F_{10}^2 and F_{10}^5, F_{20}^2 and F_{20}^5, F_{40}^2 and F_{40}^5), the corresponding PSDs almost coincide with each other. It is evident that damages on different tendons affect similarly the monitored dynamics and this indicates that damaged tendon identification and damage precise quantification are highly challenging.

3. Damaged tendon diagnosis methodology

In step 1 of the presented vibration-response-only based methodology, damage detection is achieved via a simple statistical time series method based on changes in the non-parametric PSD of vibration response signals (Fassois and Sakellariou 2009, Kopsaftopoulos and Fassois 2010). When a damage is detected, damaged tendon identification and damage precise quantification which are steps 2 and 3 are achieved based on a proper formulation of the FMBM (Sakellariou and Fassois 2008) equipped with FP-AR models. The methodology
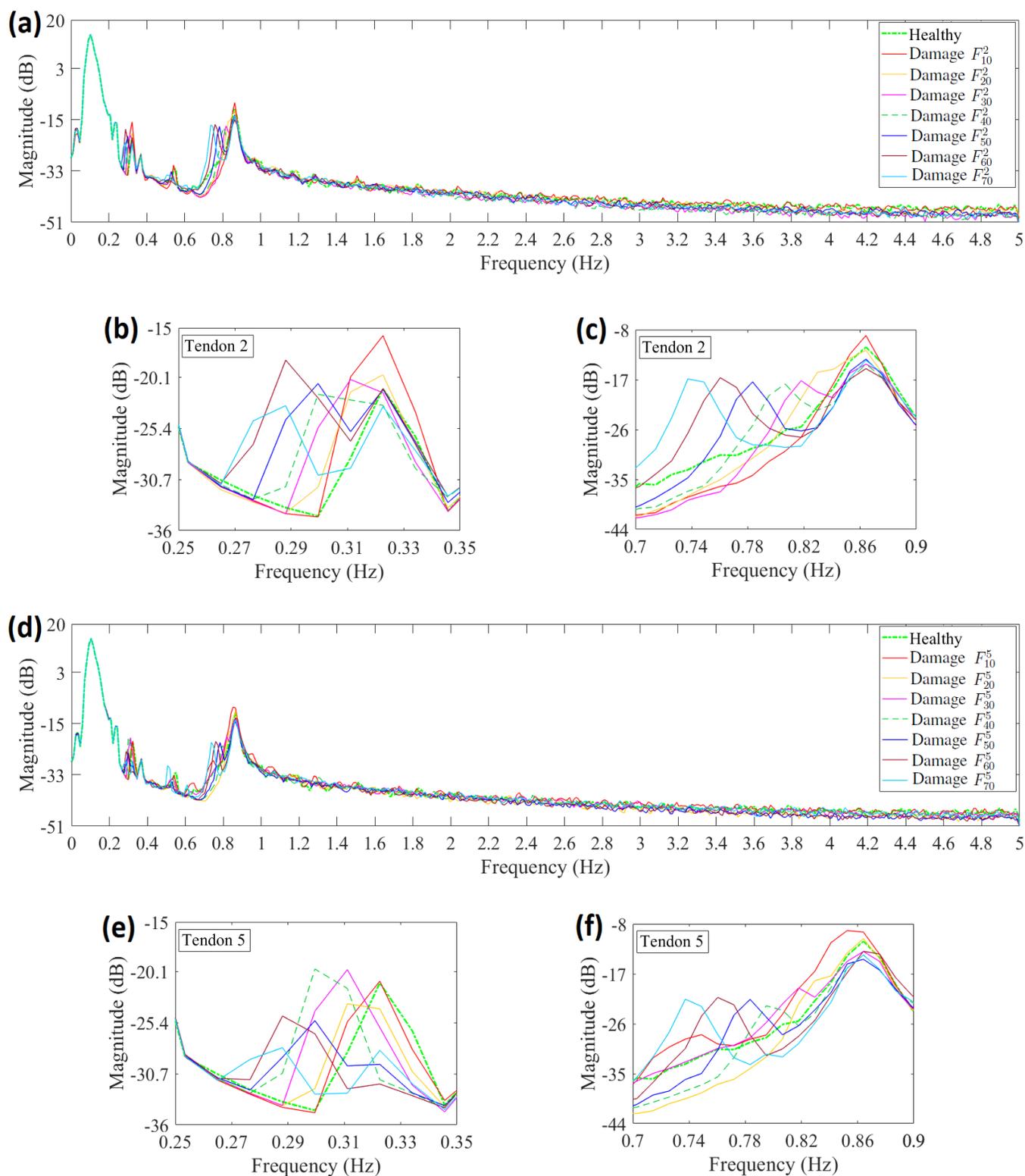
Figure 6. (a) Welch-based PSD estimates for the healthy and damaged structure under damages corresponding to F_{10}^2, F_{20}^2, F_{30}^2, F_{40}^2, F_{50}^2, F_{60}^2, and F_{70}^2. (b), (c) Blow-ups of (a). (d) Welch-based PSD estimates for the healthy and damaged structure under damages corresponding to F_{10}^5, F_{20}^5, F_{30}^5, F_{40}^5, F_{50}^5, F_{60}^5, and F_{70}^5. (e), (f) Blow-ups of (d).
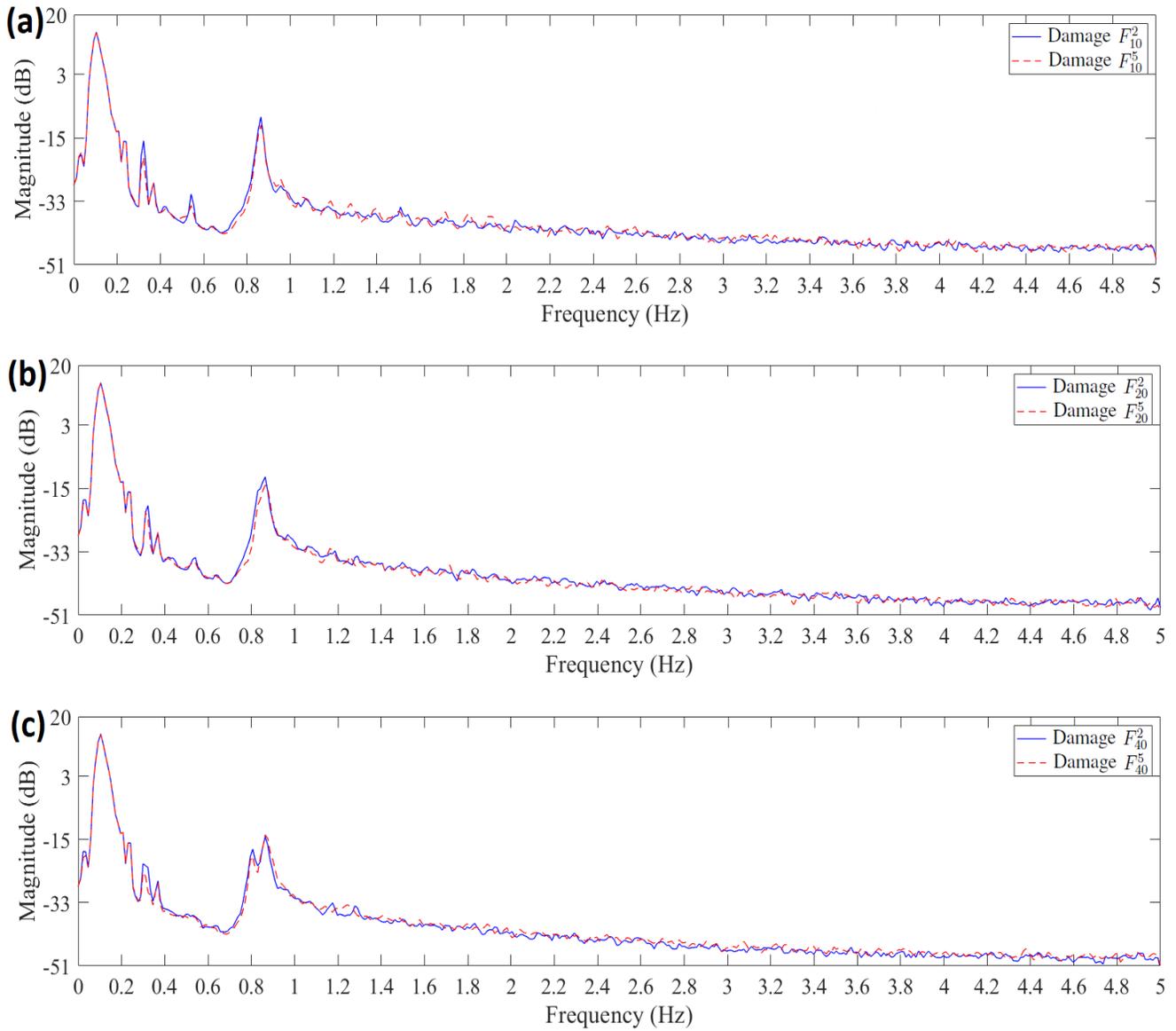
Figure 7. Comparison between Welch-based PSD estimates for damages on different tendons and of the same magnitude: (a) F_{10}^2 and F_{10}^5, (b) F_{20}^2 and F_{20}^5, (c), F_{40}^2 and F_{40}^5.

consists of two phases, the baseline phase and the inspection phase. The baseline (training) phase is performed based on data from known structural states and when the structure is not operational (shutdown condition). The inspection phase runs periodically or continuously during the structure's normal operation (on-line) based on current vibration data, while the structure is under unknown health state.

3.1 Baseline phase

A single response signal $y_o[t]$ of N samples long ($t = 1, \ldots, N$ the normalized discrete time) is acquired under the healthy structure and subsequently it is used for obtaining the PSD estimate $\widehat{S}_o(f_a)$ via the Welch estimator (a hat $\frown$ above a quantity designates its estimate).

An FP-AR model (Ahmed and Kopsaftopoulos 2017) capable of representing the FOWT platform (partial) dynamics under damage of any magnitude at the location of interest on a single tendon, is identified for each examined tendon. For the identification of an FP-AR model, M response signals are obtained for a sample of different damage magnitudes on the examined tendon. These magnitudes cover the magnitude range $[m_{min}, m_{max}]$ via the discretization $m_v \in m_1, m_2, \ldots, m_M$ and each signal is characterized by a specific magnitude m_v. Thus, for a single damage magnitude, the following operating parameter k is defined:

$$k = m_v \iff k_v \text{ with } v = 1, ., M \tag{2}$$

and a pool of M response signals $y_k[t]$, each of length N, is obtained with $t = 1, \ldots, N$.

A representation of the response signals acquirement based on damage magnitudes and of the formulation of the pool of data, is presented in Figure 8. Based on this pool of data, a mathematical description of the structural (partial) dynamics under damage of any potential magnitude on the examined tendon, is obtained through a FP-AR$(na)_p$ model of the following form:

$$y_k[t] + \sum_{i=1}^{na} \alpha_i(k) \cdot y_k[t-i] = e_k[t] \text{ with } e_k[t] \sim \text{iid } \mathcal{N}(0, \sigma_e^2(k)) \text{ and } k \in \mathbb{R} \tag{3}$$

$$a_i(k) = \sum_{j=1}^{p} a_{i,j} \cdot G_j(k) \tag{4}$$

with na designating the AutoRegressive (AR) order, $y_k[t]$ the response signal and $e_k[t]$ the disturbance (residual) signal that is white (serially uncorrelated) zero-mean with variance $\sigma_e^2(k)$. iid stands for identically independently distributed and $\mathcal{N}(:,:)$ designates normal distribution with the indicated mean and variance.

Based on Equation (4), the AR parameters $a_i(k)$ are functions of k belonging to a p-dimensional functional subspace spanned by the (mutually independent) functions $G_1(k); G_2(k); ::::; G_p(k)$ (functional basis). The latter are univariate (one variable) orthogonal polynomials (Chebyshev, Legendre, Jacobi and other families) forming a functional basis $\mathscr{G}$ (Sakellariou and Fassois 2008). The constants $a_{i,j}$ designate the AR coefficients of projection.

The FP-AR model of Equations (3) and (4) may be written in linear regression form as (bold-face upper/lower case symbols designate matrix/column-vector quantities, respectively; ^{T}designates transposition):

$$y_k[t] = [\boldsymbol{\varphi}_k^T[t] \otimes \boldsymbol{g}^T(k)] \cdot \boldsymbol{\theta} + e_k[t] = \boldsymbol{\phi}_k^T[t] \cdot \boldsymbol{\theta} + e_k[t] \tag{5}$$

with $\boldsymbol{\varphi}_k[t] = [-y_k[t-1] \ldots - y_k[t-na]]_{[na\times1]}^T$ designating the regression vector, $\boldsymbol{g}(k) = [G_1(k) \ldots G_p(k)]_{[p\times1]}^T$ the functional basis vector, $\boldsymbol{\theta} = [a_{1,1} \ldots a_{na,p}]_{[na\cdot p\times1]}^T$ the projection coefficients and $\otimes$ the Kronecker product.
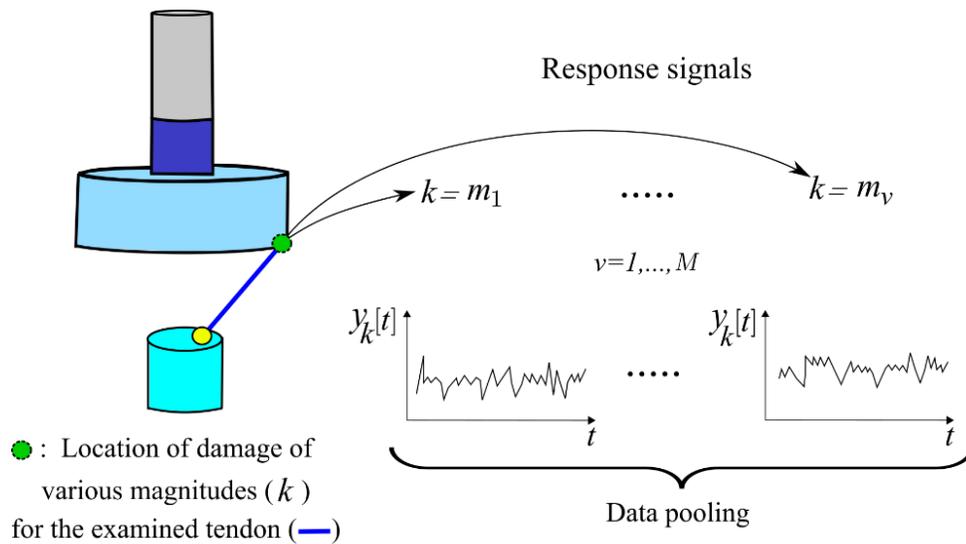
Figure 8. Representation of the response signals acquirement based on damage magnitudes and of the constructed pool of data used in the FMBM's baseline phase.

Pooling together Equation (5) of the FP-AR model corresponding to the various operating parameters $k(k_1, k_2, \ldots, k_M)$ of the obtained response signals for a single value of t, leads to:

$$
\begin{bmatrix} y_{k_1}[t] \\ \vdots \\ y_{k_M}[t] \end{bmatrix}_{[M \times 1]} = \begin{bmatrix} \boldsymbol{\phi}_{k_1}^T[t] \\ \vdots \\ \boldsymbol{\phi}_{k_M}^T[t] \end{bmatrix}_{[M \times p \cdot na]} \cdot \boldsymbol{\theta} + \begin{bmatrix} e_{k_1}[t] \\ \vdots \\ e_{k_M}[t] \end{bmatrix}_{[M \times 1]} \implies \boldsymbol{y}[t] = \boldsymbol{\Phi}[t] \cdot \boldsymbol{\theta} + \boldsymbol{e}[t] \tag{6}
$$

Then, following substitution of the data for $t = 1, \ldots, N$, the parameter vector $\boldsymbol{\theta}$ can be estimated based on the Ordinary Least Squares (OLS) estimator (Sakaris et al. 2016):

$$
\widehat{\boldsymbol{\theta}} = \left[\sum_{t=1}^{N} \boldsymbol{\Phi}^T[t] \, \boldsymbol{\Phi}[t] \right]^{-1} \cdot \left[\sum_{t=1}^{N} \boldsymbol{\Phi}^T[t] \, \boldsymbol{y}[t] \right] \tag{7}
$$

A conventional AR(*na*) model (Ljung 1999, pp. 81-83) based on a single response signal from the healthy structure, is used as a reference for the order of the FP-AR model. The AR model's order is selected through the minimization of the Bayesian Information Criterion (BIC) which is a statistical criterion that penalizes model complexity (order) as a counteraction to a decreasing quality criterion (Ljung 1999, pp. 505-507). The dimensionality of the FP-AR model's functional subspace, given a selected basis function family, is achieved via a Genetic Algorithm (GA) procedure (Haupt and Haupt 2004, pp. 27-49, Sakaris et al. 2016) based on the minimization of an extended version of the BIC (Sakellariou and Fassois 2016). It should be noted that the families of orthogonal polynomials are essentially equivalent; the main difference lies in the required number of functions for each particular case.

Finally, the validation of the FP-AR model's ability to represent the structural dynamics, is achieved through the confirmation of the uncorrelatedness (whiteness) of the model's residual signals corresponding to the M response signals. The whiteness is checked through statistical hypothesis tests such as the Pena-Rodriguez test (Peña and Rodríguez 2006) which detects changes in the partial autocorrelation function $\pi_e[\tau]$ ($\tau = 1; \ldots; h$ is the lag; Box et al. 1994, pp. 64-68) of the residual signals. The Pena-Rodriguez test is based on a D statistic which is a function of $\pi_e[\tau]$ and it follows a standard normal distribution $D \sim \mathcal{N}(0,1)$. The test is applied on each residual signal individually and a signal's whiteness is confirmed only if the absolute value of the corresponding D does not exceed the critical limit of the distribution, $|D| \leq Z_{\frac{1-\alpha}{2}}$ ($Z_{\frac{1-\alpha}{2}}$ as the critical limit,

and α as the risk level). If the whiteness is not confirmed then the residual signal is considered nonwhite and the FP-AR model is not able to represent the structural dynamics.

3.2 Inspection phase

Step 1: Damage detection. A response $y_u[t]$ signal is obtained from the current (unknown) health state of the structure and it is used for obtaining the Welch-based PSD estimate $\widehat{S}_u(f_a)$. Then damage detection is accomplished by comparing the current $\widehat{S}_u(f_a)$ to its healthy (baseline) counterpart $\widehat{S}_o(f_a)$ through a binary hypothesis test. A deviation from the baseline PSD indicates the presence of damage. This test is based on an F statistic (F$= \widehat{S}_o(f_a)/\widehat{S}_u(f_a)$) following a Fischer distribution (denoted by F) with $(2Q, 2Q)$ degrees of freedom, F$\sim F_{2Q,2Q}$ (Q is the number of windows used in the Welch estimator and it is equal to the signal length divided by the window length; Fassois and Sakellariou 2009, Kopsaftopoulos and Fassois 2010). A damage is detected if the F statistic exceeds any of the critical limits of the distribution, F$\leq -f_{\frac{1-\alpha}{2},2Q,2Q}$, F$\geq f_{\frac{1-\alpha}{2},2Q,2Q}$ with - $f_{\frac{1-\alpha}{2};2Q;2Q}$ and $f_{\frac{1-\alpha}{2};2Q;2Q}$ the critical limits and α the risk level. If the F statistic does not exceed the critical limits then the examined structure is considered healthy.

Step 2: Damaged tendon identification. If a damage is detected, then the signal $y_u[t]$ is driven through each (baseline phase) FP-AR model (one model per examined tendon) which is now re-parametrized in terms of the currently unknown $k = m$:

$$y_u[t] + \sum_{i=1}^{na} a_i(k) \cdot y_u[t-i] = e_u[t,k] \tag{8}$$

The estimation of k is achieved based on the following Nonlinear Least Squares (NLS) estimator (realized via golden search and parabolic interpolation; Forsythe et al. 1976, pp. 178-184):

$$\widehat{k} = \arg\min_{k \in K} \sum_{t=1}^{N} e_u^2[t,k], \qquad \widehat{\sigma}_{e_u}^2 = \frac{1}{N} \sum_{t=1}^{N} e_u^2[t,\widehat{k}] \tag{9}$$

with $e_u[t, k]$ provided by Equation (8), $K = [k_{min}, k_{max}]$ and k_{min}, k_{max} the boundaries of the examined magnitude range m_{min}, m_{max}. The estimate $\widehat{k}$ is asymptotically ($N \to \infty$) normally distributed with mean μ_k and variance σ_k^2, that is $\widehat{k} \sim \mathcal{N}(\mu_k, \sigma_k^2)$.

The validity of the estimate $\widehat{k}$ based on the FP-AR model for the examined tendon, is accepted only when the uncorrelatedness (whiteness) of the residual signal $e_u[t, \widehat{k}]$ is confirmed via the Pena-Rodriguez test (Sakaris et al. 2016). The whiteness of the residual signal is confirmed only if the ¡D¡ statistic does not exceed the critical limit of the normal distribution (see section 3.1). The acceptance of the validity means that the FP-AR model is able to represent the structural dynamics under the current damage and that the examined tendon is identified as the damaged tendon. It should be noted that if the above procedure underlines that the estimate $\widehat{k}$ belongs to two or more tendons, the one with the lowest ¡D¡ statistic is selected as the actual damaged tendon. If $e_u[t, \widehat{k}]$ is not white then an alternative FP-AR model (representing a different tendon) shall be checked.

Step 3. Damage precise quantification. If the examined tendon has been successfully identified as the damaged tendon, then the estimate $\widehat{k}$ is accepted as the estimated magnitude of the damage corresponding to the identified damaged tendon. Then, a confidence interval for $\widehat{k}$ is constructed (Sakellariou and Fassois 2008):

$$\left[\widehat{k} - t_{1-\frac{\alpha}{2}, N-1} \cdot \widehat{\sigma}_k, \ \widehat{k} + t_{1-\frac{\alpha}{2}, N-1} \cdot \widehat{\sigma}_k \right] \tag{10}$$

with $-t_{1-\frac{\alpha}{2}, N-1}$ and $t_{1-\frac{\alpha}{2}, N-1}$ designating the t distribution's (with $N-1$ degrees of freedom) critical limits, α the risk level and $\widehat{\sigma}_k$ the standard deviation of $\widehat{k}$ provided by the Cramer-Rao lower bound (Sakellariou and Fassois 2008).

A flowchart of the aforementioned methodology is presented in Figure 9.
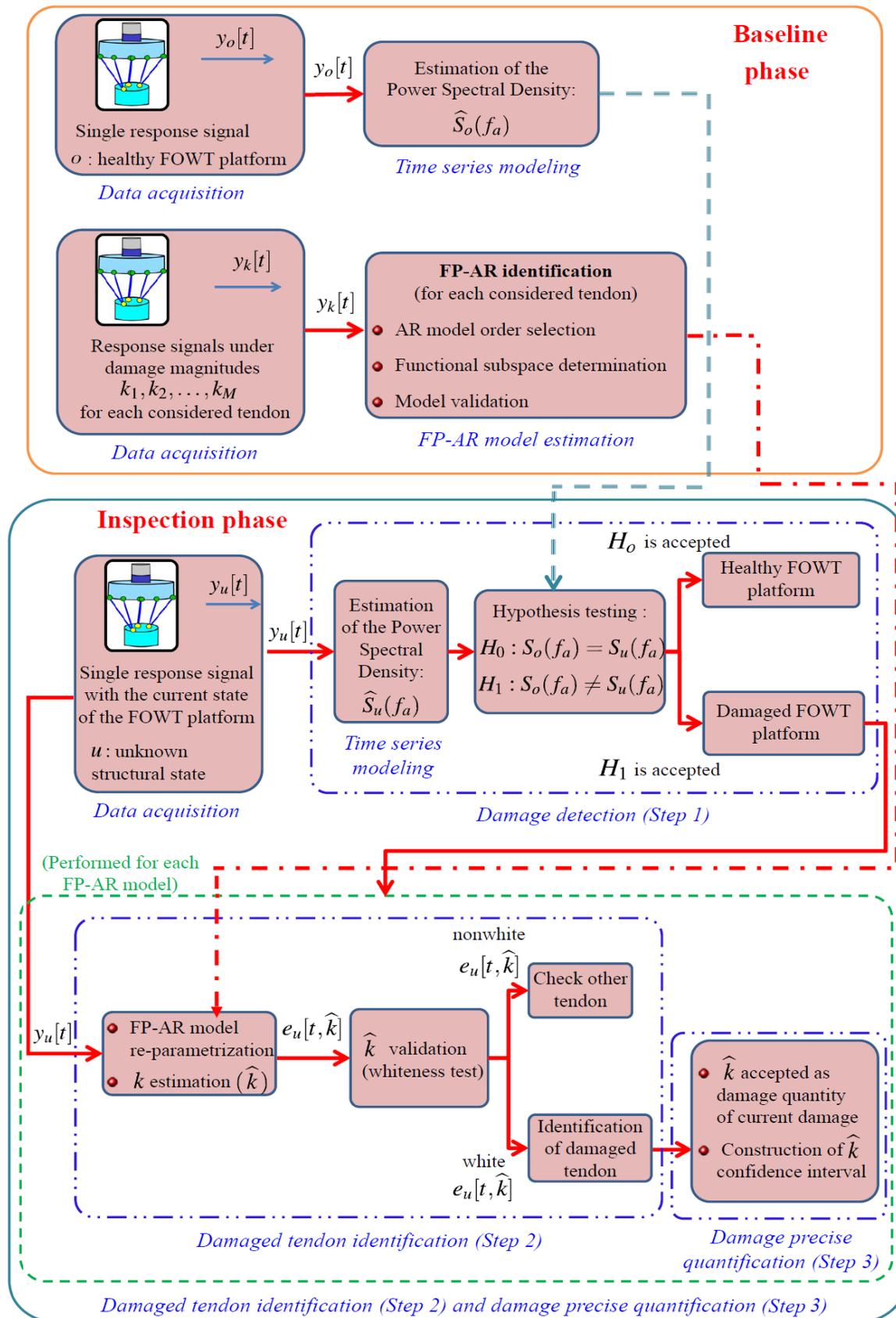
Figure 9. Flowchart of the damaged tendon diagnosis methodology.

4. Damaged tendon diagnosis methodology

4.1 Baseline phase

The PSD estimate $\widehat{S}_o(f_a)$ of a response signal from the healthy structure is obtained based on the Welch estimator. For the proper selection of the risk level corresponding to the thresholds of the hypothesis test in the PSD based method, the following procedure is adopted. A PSD is additionally estimated based on a different response signal from the healthy structure and subsequently based on each of 20 response signals from various damaged states (one signal per state). The hypothesis testing procedure is applied on each pair of PSDs consisting of the PSD $\widehat{S}_o(f_a)$ and one of the 21 additional PSDs. Thus, the method's risk level and the critical limits (thresholds) are selected so that the $\widehat{S}_o(f_a)$ and the additional PSD from the same healthy state appearing as statistically identical while the $\widehat{S}_o(f_a)$ and the PSD from a damage state appearing as statistically different. The selected statistical limits are then employed throughout the inspection phase. The method's details are provided in Table 2. A typical computer (Intel Core(TM) i5-7600 CPU @ 3.5 GHz, 8 GB RAM, Windows 10 Enterprise Operating System) is used throughout the baseline and inspection phases. The time needed for the estimation of a PSD model is 0.007 seconds (see Table 3).

Table 2. PSD estimation details and PSD based method results.

Baseline phase

Signal length	No. of signals	Window length	Window type	Frequency resolution
N=20000 samples	22	868 samples	Hamming	Δf=0.011 Hz

Estimation method: Welch estimator; Matlab function: *pwelch.m*

Damage detection: Risk level: $\alpha = 1 \cdot 10^{-6}$

Inspection phase – Step 1: Damage detection

False Alarms	Missed Damages
0/3 (100%)	0/108 (100%)

Table 3. Completion time of various tasks of the damaged tendon diagnosis methodology.

Baseline phase

Tendon	Model	Task	Completion time
-	PSD	Model estimation	0.007 seconds
-	AR(140)	Model estimation	23 seconds
2	FP-AR$(140)_4$	Functional subspace determination	21 minutes
5	FP-AR$(140)_7$	Functional subspace determination	28 minutes

Matlab functions: *clock.m, etime.m*

Computer: *Intel Core(TM) i5-7600 CPU @ 3.5 GHz, 8 GB RAM, Windows 10 Enterprise Operating System*

Inspection phase

Task	Completion time per damage scenario
Step 1: Damage detection	0.001 seconds
Step 2: Damaged tendon identification	3.5 – 7.5 seconds
Step 3: Damage precise quantification	0.1 seconds

Matlab functions: *clock.m, etime.m*

Computer: *Intel Core(TM) i5-7600 CPU @ 3.5 GHz, 8 GB RAM, Windows 10 Enterprise Operating System*

Then for each examined tendon, a number of $M = 10$ response signals are used for the identification of an FP–AR model representing the structural dynamics under any damage magnitude on the tendon in the damage magnitude range $m_v \in [10, 100]\%$ (see section 3.1). The range is covered via the discretization $m_v \in [10, 20, 30, \ldots, 80, 90, 100]\%$. The AR model order is selected to be identical to that of a conventional AR(140) model identified based on a response signal from the healthy structure (see Table 4 for details). The orders of the conventional model are selected based on the BIC minimization (Table 4) and it is subsequently validated via a combination of tools. These tools include a residual whiteness test based on the autocorrelation function of the residual signal (Ljung 1999, pp. 512-513) and a stabilization diagram which depicts the estimated modal parameters (usually frequencies) as a function of increasing model order (Fassois 2001, Kopsaftopoulos and Fassois 2010). 23 seconds are needed for the estimation of the AR(140) model (see Table 3). Then the dimensionality of the FP–AR model's functional subspace is determined via a GA-based procedure based on the minimization of BIC. The initial functional subspace is selected to be spanned by 10

univariate Shifted Legendre polynomials which are functions of the damage magnitude m_v normalized with respect to the maximum value that is $m_v = m_v/100 \in [0, 1]$.

Two models, an FP-AR$(140)_4$ and an FP-AR$(140)_7$, are identified for tendons 2 and 5, respectively. A comparison between the Welch-based (Welch estimation details: Matlab function *pwelch.m*; signal length 20000 samples, window 868 samples, 95 % overlap, Hamming window, frequency resolution of 0.011 Hz) and the FP-AR models' PSD estimates, is presented in Figure 10. Their agreement shows the excellent modeling of the damaged structural dynamics based on the FP-AR models. Finally, by applying the Pena-Rodriguez test on the residual signals of the FP-AR models, the risk levels and thus the critical limits are selected such that both of the FP-AR models remain valid. The critical limits are then employed throughout the inspection phase. Full details on the FP-AR models identification, are presented in Table 4. The time needed in the determination of the FP-AR models functional subspace, is 21 minutes for the FP-AR$(140)_4$ model and 28 minutes for the FP-AR$(140)_7$ model (Table 3).
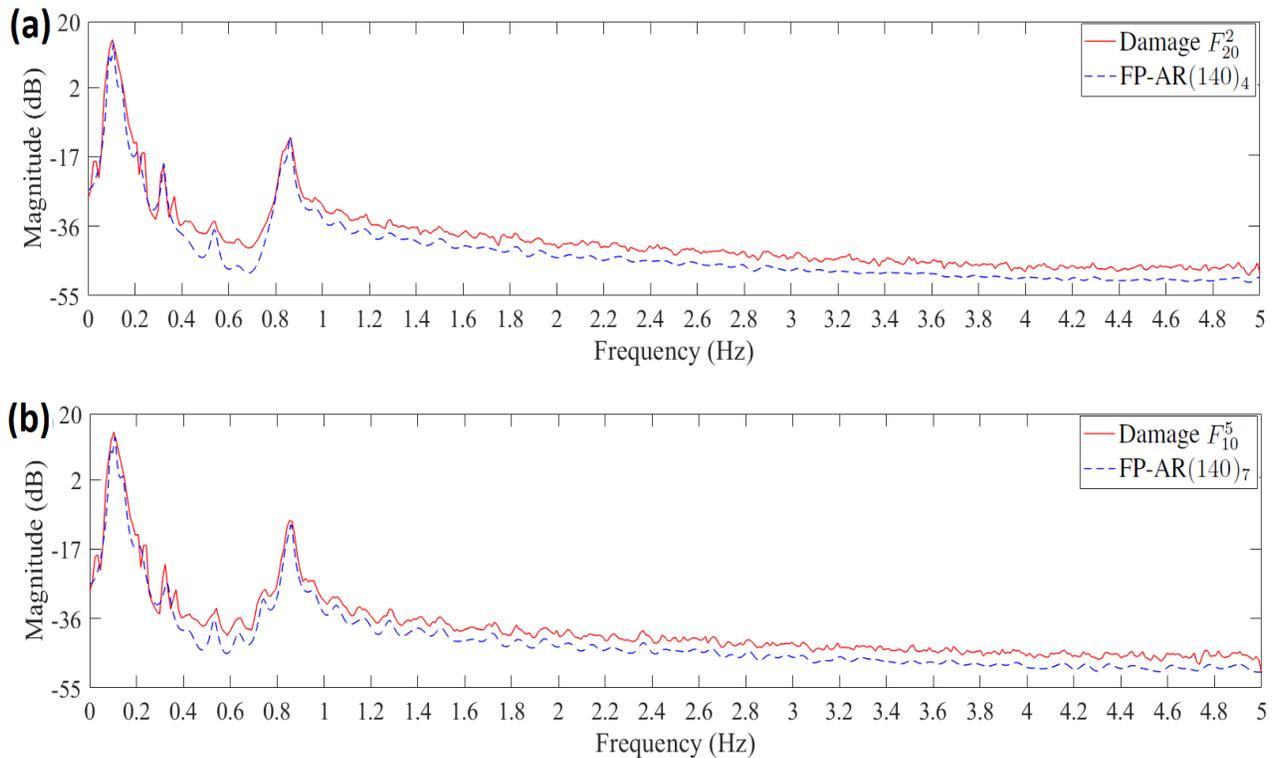
Figure 10. (a) Welch based PSD estimate (——) for damage F_{20}^2 and the FP-AR$(140)_4$ model's PSD estimate (– – –); (b) Welch based PSD estimate (——) for damage F_{10}^5 and the FP-AR$(140)_7$ model's PSD estimate.

Table 4. Details of the FMBM.

Baseline phase

State	Tendon	Signal length	Estimated model	No. of signals	No. of projection coefficients	Sample per Parameter	Condition number[a]	BIC
Healthy	-	N=20000 samples	AR(140)	$M = 1$	-	142.85	$5.95 \cdot 10^5$	-7.3
Damaged	2	N=20000 samples	FP-AR$(140)_4$	$M = 10$	560	357.14	$9.28 \cdot 10^6$	-75.71
Damaged	5	N=20000 samples	FP-AR$(140)_7$	$M = 10$	980	204.08	$3.37 \cdot 10^7$	-72.08

Order selection based on an AR model: Estimation method*:* OLS, Matlab function: *arx.m*

Functional subspace dimensionality determination based on Genetic Algorithm: population=100, elite count 20, crossover fraction=0.7, maximum number of generations=100, Tolerance of the objective function $= 10^{-10}$; Matlab function: *ga.m*

FP-AR(140)₄ model's functional basis: p=4 univariate Shifted Legendre polynomials: $\mathscr{G} = [G_0(k) \ G_1(k) \ G_3(k) \ G_5(k)]^b$

FP-AR(140)₇ model's functional basis: p=7 univariate Shifted Legendre polynomials:
$\mathscr{G} = [G_0(k) \ G_1(k) \ G_2(k) \ G_3(k) \ G_4(k) \ G_6(k) \ G_8(k)]^b$

Validation method: Pena-Rodriguez test with risk levels $\alpha = 7.05 \times 10^{-1}$ (FP-AR$(140)_4$ model), $\alpha = 6.08 \times 10^{-1}$ (FP-AR$(140)_7$ model) & no. of lags = 28

Inspection phase – Step 2: Damaged tendon identification & Step 3: Damage precise quantification

FP-AR models based estimation of k: NLS estimator based on golden search & parabolic interpolation (Tolerance of the objective function $= 10^{-10}$; Tolerance of the estimated value $= 10^{-10}$; Matlab function: *fminbnd.m*)

Validation method: Pena-Rodriguez test with risk levels $\alpha = 7.05 \times 10^{-1}$ (FP-AR$(140)_4$ model), $\alpha = 6.8 \times 10^{-1}$ (FP-AR$(140)_7$ model) & no. of lags = 28

[a] Condition number of $\sum_{t=1}^{N} \mathbf{\Phi}^T[t] \mathbf{\Phi}[t]$ in Equation (7); [b] $G_i(k)$: univariate orthogonal polynomial of degree i

4.2 Inspection phase

Step 1: Damage detection. Indicative damage detection results are provided in Figure 11. It is evident that detection without false alarm or missed damage is achieved at $\alpha = 1 \cdot 10^{-6}$ in each scenario as the ꜰ statistic does not exceed the critical limits in the healthy state and it exceeds any of the limits in the damaged states (see section 3.2). It must be noted that the damages F_{15}^2 , F_{25}^2, F_{25}^5 are hardest to detect as the F statistic is within the critical limits for most frequencies. This happens because these damages have minor effects on the

platform dynamics due to the tendons' high strength (see section 2.4). The damages F_{35}^2, F_{45}^2, F_{55}^2, F_{65}^2, F_{35}^5, F_{45}^5, F_{55}^5, F_{65}^5, F_{75}^5 are easiest as the F statistic exceeds the critical limits for multiple frequencies. The critical limits are exceeded in the bandwidths of [0.27-0.35] Hz and [0.7-0.9] Hz. In some damages, there is an additional exceedance in the bandwidth of [0.5-0.6] Hz. A summary of all damage detection results based on the 3 healthy and 108 damage scenarios corresponding to simulations (response signals) exclusively used in the inspection phase, is presented in Table 2. The time needed for the completion of damage detection per damage scenario is 0.001 seconds (Table 3).
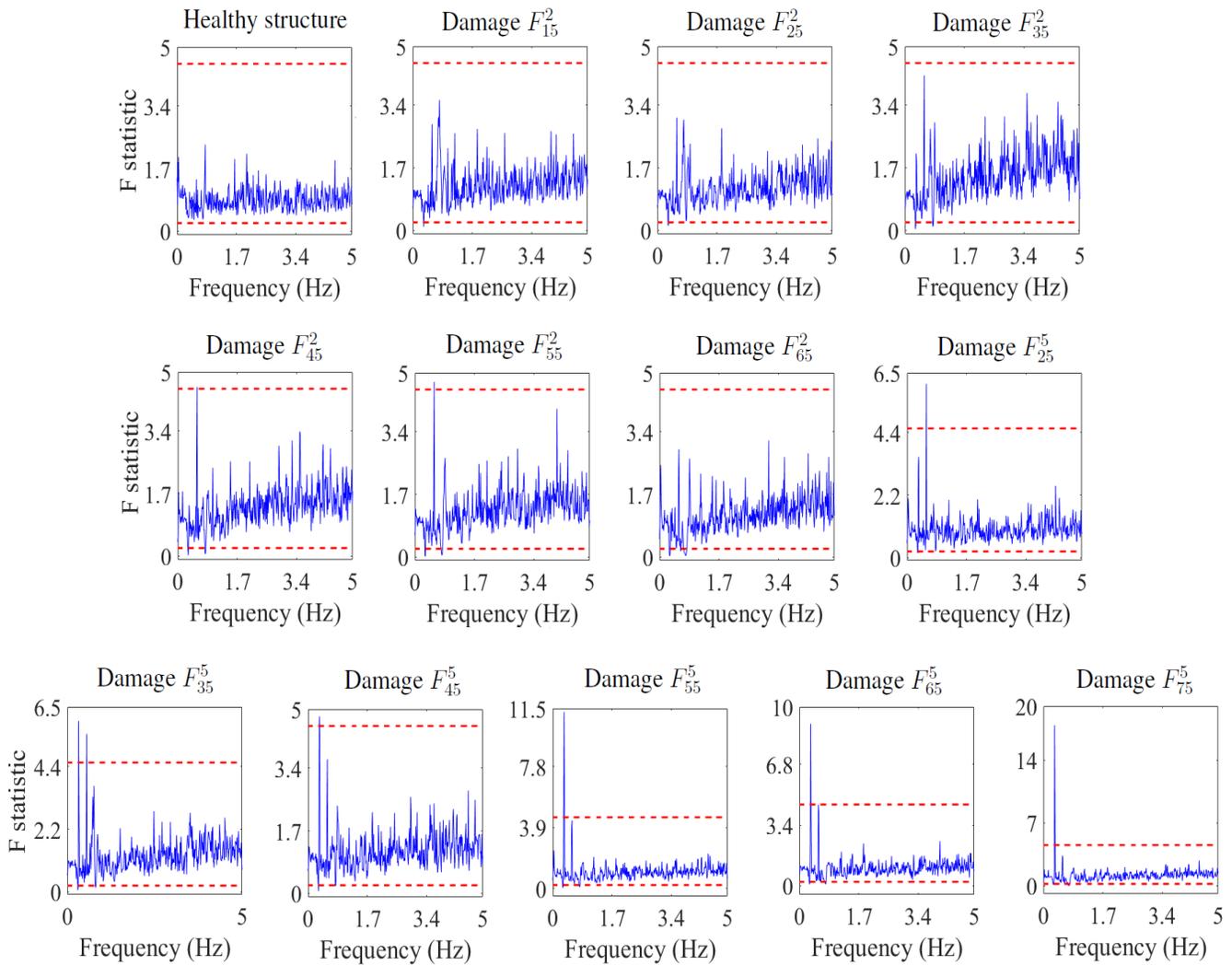
Figure 11. Indicative damage detection results for 1 healthy and 12 damage scenarios through the PSD based method. The actual structural state is shown above each plot and the critical limits are represented as dashed horizontal lines.

Step 2: Damaged tendon identification. Once a damage is detected, damaged tendon identification is activated. Each considered baseline FP-AR model is re-parametrized in terms of the k corresponding to the unknown (current) damage (Equation (8)). Based on each re-parametrized model, the NLS estimator of Equation (9) searches for the estimate $\widehat{k}$ thus leading to the minimum of the estimation criterion (see details in Table 4). Then the damaged tendon is identified through the ¡Dj statistic based on the partial autocorrelation of $e_u[t, \widehat{k}]$ (Matlab function: *parcocorr.m*; see Section 3.2 and Table 4).
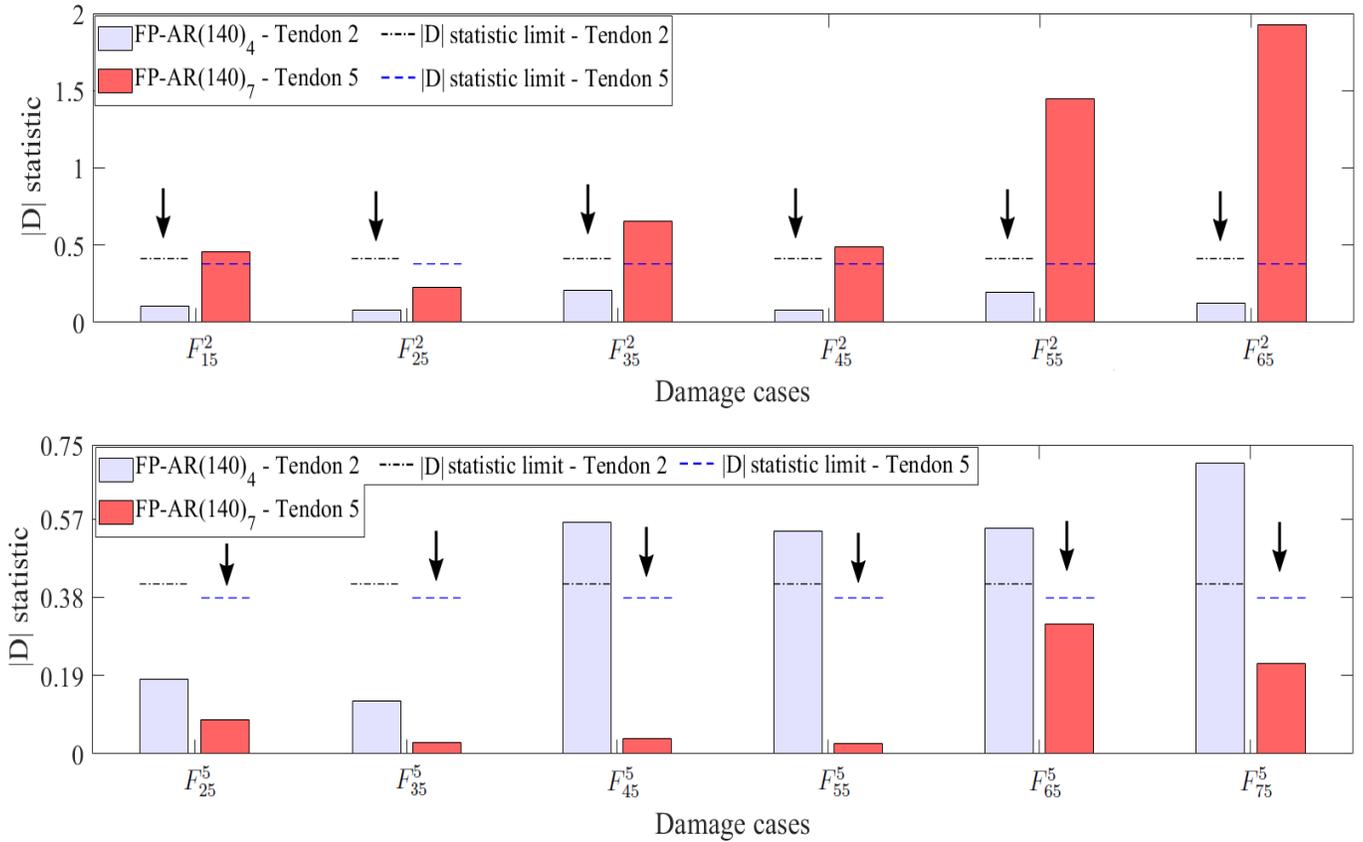
Figure 12. Indicative damaged tendon identification results for 12 damage scenarios. The actual structural state is shown below each pair of bars. The dark arrow shows the tendon selected as the actual damaged tendon in each scenario.

Indicative damaged tendon identification results achieved at $\alpha = 7.05 \times 10^{-1}$ for the FP-AR$(140)_4$ model of tendon 2 and at $\alpha = 6.08 \times 10^{-1}$ for the FP-AR$(140)_7$ model of tendon 5, are provided in Figure 12. It is evident that damaged tendon identification is achieved when only the ¡Dj statistic of the model based on the actual damaged tendon does not exceed the corresponding critical limit. In some damages such as

F_{25}^2, F_{25}^5, and F_{35}^5, the ¡Dj statistics of both models don't exceed the corresponding critical limits. This happens

because these damages affect similarly the platform dynamics (see Section 2.4). Thus, the lowest ¡Dj statistic

is selected and it leads to the actual damaged tendon. Damaged tendon identification is achieved in all of the

108 considered damage scenarios and a summary of the corresponding results is provided in Table 5. The time

needed for damaged tendon identification per damage scenario is 3.5 to 7.5 seconds (Table 3). *Step 3. Damage*

precise quantification. After the identification of the damaged tendon, the corresponding estimate $\widehat{k}$ (Equation

(9)) is accepted and the confidence interval is constructed (Equation (10)).

Table 5. Damaged tendon identification and damage precise quantification results

Step 2: Damaged tendon identification			Step 3: Damage precise quantification
Tendon	Model	Identification	Quantification error δk (sample mean $\pm$ std)
2	FP-AR$(140)_4$	54/54 (100 %)	1.43 + 1.44 (%)
5	FP-AR$(140)_7$	54/54 (100 %)	2.41 $\pm$ 2.94 (%)

Indicative damage precise quantification results in terms of damage magnitude estimates and confidence

intervals are provided in Figure 13. It is evident that damage precise quantification is achieved at $\alpha = 1 \times 10^{-6}$

as the estimated and the actual damage magnitudes are very close with the latter being within or just outside

of the obtained confidence intervals. A summary of all damage precise quantification results based on the 108

considered damage scenarios, is presented in Figure 14 and in Table 5. The quantification error δk which is

the error between the actual (k) and its estimated damage magnitude $(\widehat{k})$, is provided in Figure 14. δk remains

smaller than 5 % for 94.44 % of the 54 damage scenarios based on tendon 2 and for 83.33 % of the 54 damage

scenarios based on tendon 5. The maximum quantification error is 10.5 % which is quite small for large

structures such as the FOWT platform. The mean quantification errors are 1.55 % for tendon 2 and 2.49 % for

tendon 5 (see Table 5). The time needed for damage precise quantification per damage scenario is 0.1 seconds

(Table 3).
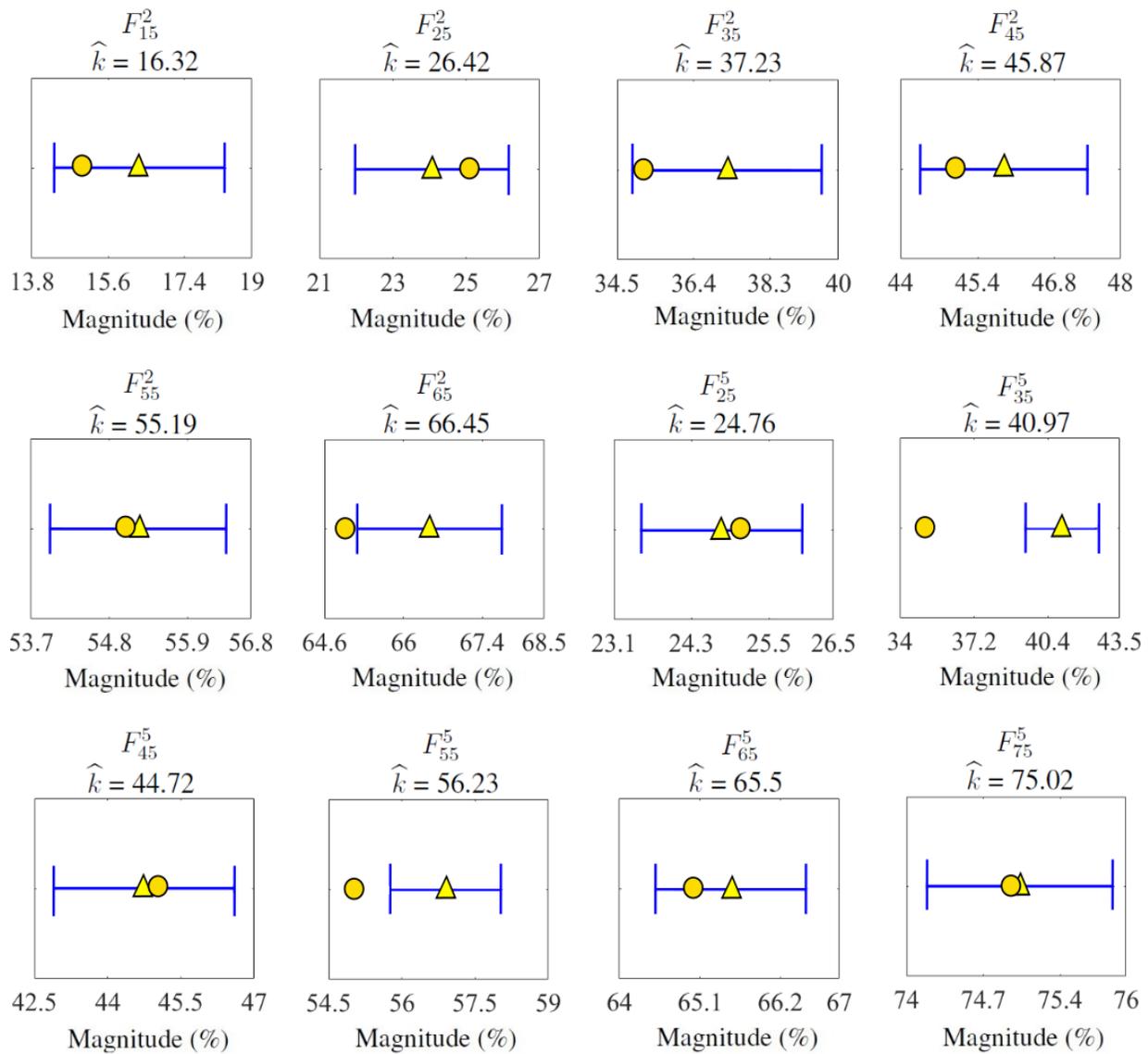
Figure 4. Indicative damage precise quantification results for 12 damage scenarios (⭕ : true damage magnitude; △ : point estimate; ⊢⊣ : confidence interval). The true and estimated damage magnitude are numerically provided above each plot.
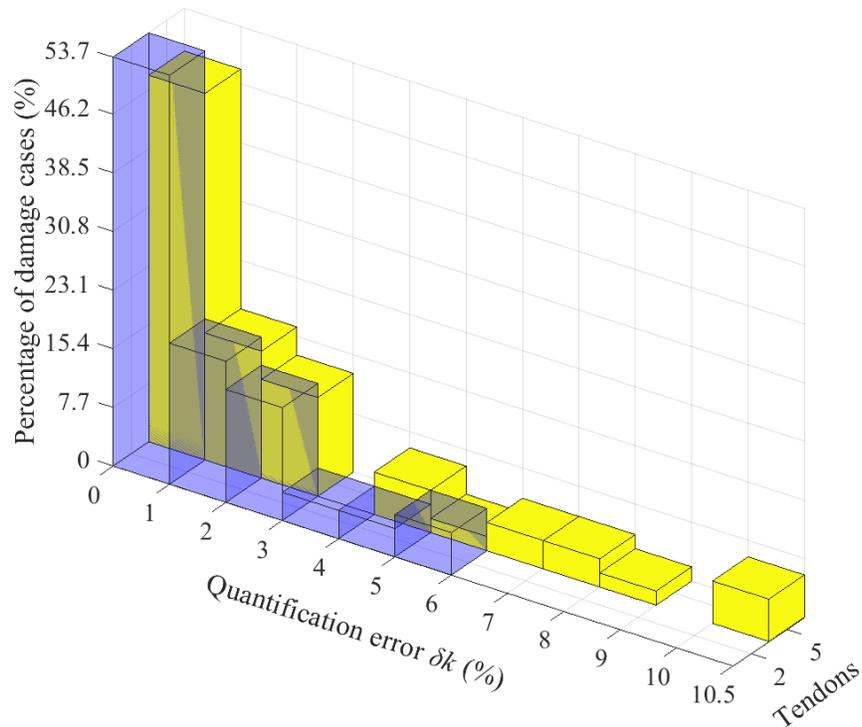
Figure 5. Damage precise quantification results in terms of the quantification error δk (%) which is the error between the actual and its estimated damage magnitude (54 damage scenarios based on tendon 2 and 54 damage scenarios based on tendon 5).

5. Conclusions

The problem of damaged tendon diagnosis (damage detection, damaged tendon identification and damage precise quantification) on a new 10 MW multibody FOWT platform was for the first time explored via the PSD-based method and the stochastic FMBM. The latter was appropriately formulated in this study to operate with only vibration response signals. The diagnosis was achieved using vibration response (acceleration) signals from the platform's healthy and damaged states. The signals were obtained from a coupled numerical model describing the platform's dynamics. Due to the current study being an early study on damaged tendons on a 10MW multi-body platform and the investigation of the platform under parked conditions only, the bodies were subjected only to current and irregular wave excitation loads. The examined damage scenarios corresponding to the stiffness reduction of two different tendons, at the connection points to the upper tank of the platform were investigated. The study included damages corresponding to a stiffness reduction of [10-25]

% with minor effects on the platform's dynamics due to the tendons high strength and damages corresponding to a stiffness reduction of [10-85] % with similar effects on the dynamics. Thus, the diagnosis capability of the presented methodology was tested under highly challenging conditions. Practical constraints were also investigated in this study, through the use of a single underwater accelerometer on the upper tank of the platform and a low and limited frequency bandwidth (0-5 Hz) of surge acceleration signals. The main conclusions of the study are summarized as follows:

- Accurate modeling of the structural dynamics under any damage magnitude on the examined tendons and all considered current-wave excitation loads was achieved based on response-only FP-AR models.

- Damage detection was perfectly accomplished using the PSD-based method in all the considered damage scenarios without cases of missed damages or false alarms.

- Damaged tendon identification via the FMBM was conducted successfully in all the examined cases.

- Damage precise quantification via the FMBM was very accurate with the actual damage being in all the examined cases within or just outside the obtained confidence intervals.

- Damaged tendon diagnosis was achieved in the inspection phase very quickly with the required time being less than 7.6 seconds in all examined cases.

- Overall, damaged tendon diagnosis on multibody type of offshore platforms is possible via advanced vibration-based methods equipped with data-based models. Although, it should be noted that improved damage quantification results are expected if the FMBM is based on signals from more than a single sensor and degree of freedom.

- The mooring lines integrity is equally important as the tendons integrity, for the 10 MW multibody FOWT platform's stability and thus a future work on damaged mooring line diagnosis in the platform, is expected.

- As a multibody offshore platform subjected only to current and wind loads was considered in this study, a new study on damaged tendon diagnosis in the10 MW FOWT added on the multibody platform under varying current, wave and wind loads, is already under preparation.

Acknowledgement

References

Ahmed, S., Kopsaftopoulos, F., 2017. Investigation of broadband high-frequency stochastic actuation for active-sensing SHM under varying temperature. In: Proceedings of the 12th International Workshop on Structural Health Monitoring (IWSHM). Stanford, USA.

Armesto, J.A., Jurado, A., Guanche, R., Couñago, B., Urbano J., Serna, J., 2018. TELWIND: Numerical Analysis of a Floating Wind Turbine Supported by a Two Bodies Platform. In: Proceedings of the 37th International Conference on Ocean, Offshore and Arctic Engineering (OMAE). Madrid, Spain. Vol. 10, p. V010T09A073.

Begg, S.E., Fowkes, N., Stemler, T., Cheng, L., 2018. Fault detection in vibration systems: Identifying damaged moorings. Ocean Engineering. 164, 577-589.

Box, G.E.P., Jenkins, G.M., Reinsel, G.C., 1994. Time series analysis: Forecasting and control. Prentice-Hall, New Jersey. 3rd edition.

Chandrasekaran, S., Chithambaram, T., 2018. Structural health monitoring of offshore buoyant leg storage and regasification platform: Experimental investigations. Journal of Marine Science and Applications. 17, 87-100.

Chandrasekaran, S., Chithambaram, T., 2019. Health monitoring of tension leg platform using wireless sensor

networking: experimental investigations. Journal of Marine Science and Technology. 24, 60-72.

Chakrabarti, S.K., 2005. Handbook of offshore engineering. Elsevier, London. 1st edition.

Chen, L., Basu, B., Nielsen, R.K., 2018. A coupled finite difference mooring dynamics model for floating offshore wind turbine analysis. Ocean Engineering. 162, 304-315.

Chen, L., Basu, B., 2019. Wave-current interaction effects on structural responses of floating offshore wind turbines. Wind Energy. 22(2), 327-339.

Ettefagh, M.M., 2015. Damage identification of a TLP floating wind turbine by meta-heuristic algorithms. Chinese Ocean Engineering. 29(6), 891-902.

Faltinsen, O.M., 1990. Sea loads on ships and offshore structures. Cambridge University Press, Cambridge.

Fassois, S.D, Sakellariou, J.S., 2009. Statistical time series methods for structural health monitoring, In C. Boller, F. K. Chang & Y. Fujino (eds.), Encyclopedia of structural health monitoring: 443-472. John Wiley & Sons, Chichester.

Forsythe, G.E., Malcolm, M.A., Moler C.B., 1976. Computer methods for mathematical computations. Prentice-Hall, NewJersey.

Haupt, R.L., Haupt, S.E., 2004. Practical genetic algorithms. John Wiley & Sons, New Jersey. 2nd edition.

Jahangiri, V., Mirab, H., Fathi, R., Ettefagh, M.M., 2016. TLP structural health monitoring based on vibration signal of energy harvesting system. Latin American Journal of Solids and Structures. 13(5), 897-915.

Jamalkia, A., Ettefagh, M.M., Mojtahedi, A., 2016. Damage detection of TLP and Spar floating wind turbine using dynamic response of the structure. Ocean Engineering. 125, 191-202.

Journee, J.M.J., Massie, W.W., 2001. Offshore hydromechanics. Delft University of Technology, Delft. 1st edition.

Kopsaftopoulos, F.P., Fassois, S.D., 2010. Vibration based health monitoring for a lightweight truss structure: Experimental assessment of several statistical time series methods. Mechanical Systems and Signal Processing.

24(7), 1977-1997.

Kopsaftopoulos, F.P, Fassois, S.D., 2013. A functional model based statistical time series method for vibration based damage detection, localization, and magnitude estimation. Mechanical Systems and Signal Processing. 39(1-2), 143-161.

Ljung, L., 1999. System identification: Theory for the user. Prentice Hall, New Jersey. 2nd edition.

Peña, D., Rodríguez, J., 2006, The log of the determinant of the autocorrelation matrix for testing goodness of fit in time series, Journal of Statistical Planning and Inference.136(8), 2706-2718.

Ren, P., Zhou, Z., 2012. A state-of-the-art review on structural health monitoring of deepwater floating platform. Pacific Science Review. 14(3), 253-263.

Sakaris, C.S., Sakellariou, J.S., Fassois, S.D., 2015. Vibration-based damage precise localization in three-dimensional structures: Single versus multiple response measurements. Structural Health Monitoring. 14(3), 300-314.

Sakaris, C.S., Sakellariou, J.S., Fassois, S.D., 2016. A time series generalized functional model based method for vibration-based damage precise localization in structures consisting of 1D, 2D and 3D elements. Mechanical Systems and Signal Processing. 74, 199-213.

Sakaris, C.S., Sakellariou, J.S., Fassois, S.D., 2017a. Random-vibration-based damage detection and precise localization on a lab-scale aircraft stabilizer structure via the Generalized Functional Model Based Method. Structural Health Monitoring. 16(5), 594-610.

Sakaris, C.S., Sakellariou, J.S., Fassois, S.D., 2017b. Vibration-based multi-site damage precise localization via the Functional Model Based Method. In: Proceedings of the X International Conference on Structural Dynamics. Rome, Italy. Procedia Engineering. 199, 2072-2077.

Sakellariou, J.S., Fassois, S.D., 2008. Vibration based fault detection and identification in an aircraft skeleton structure via a stochastic functional model based method. Mechanical Systems and Signal Processing. 22(3), 557-573.

Sakellariou, J.S., Petsounis, K.A., Fassois, S.D., 2015. Vibration based fault diagnosis for railway vehicle suspensions via a functional model based method: A feasibility study. Journal of Mechanical Science and Technology volume. 29, 471–484.

Sakellariou, J.S., Fassois, S.D., 2016. Functionally Pooled models for the global identification of stochastic systems under different pseudo-static operating conditions. Mechanical Systems and Signal Processing. 72-73, 785-807.

Sakellariou, J.S., Fassois, S.D., 2017. Global identification of stochastic dynamical systems under different pseudo-static operating conditions: The functionally pooled ARMAX case. Mechanical Systems and Signal Processing. 82, 32-55.

Sakellariou, J.S., Fassois, S.D., Sakaris, C.S., 2018. Vibration-based damage localization and estimation via the stochastic Functional Model Based Method (FMBM) - an overview. Structural Health Monitoring. 17(6), 1335-1348.

Stoica, P., Moses, R., 1997. Introduction to spectral analysis. Prentice-Hall, New Jersey.

Tang, D., Chen, J., Wu, W., Jin, L., Yu, Q., Xie, B., Wang, S., Feng, J., 2020. Research on sampling rate selection of sensors in offshore platform shm based on vibration. Applied Ocean Research. 101, 102192.

Wang, P., Tian, X., Peng, T., Luo, Y., 2018. A review of the state-of-the-art developments in the field monitoring of offshore structures. Ocean Engineering. 147, 148-164.

Yang, Y., Bashir, M., Wang, J., Michailides, C., Loughney, S., Hernandez, S., Urbano, J., Armin, M., Chun, L., 2020a. Wind-wave coupling effects on the fatigue damage of tendons for a 10 MW multi-body floating wind turbine. Ocean Engineering. 217, 107909.

Yang, Y., Bashir, M., Michailides, C., Wang, J., 2020b. Development and application of an aero-hydro-servo-elastic coupling framework for analysis of floating offshore wind turbines. Renewable Energy. 261, 606-625.